Supporting Information

Charge Transfer Modulated Heterointerface for Hydrogen Production at All pH

Mamoni Maji,[1]§ Nikalabh Dihingia,[1]§ Supriti Dutta,[2] Sahanaz Parvin,[1] Swapan K. Pati,[2] and Sayan Bhattacharyya[1,]*

[1]*Department of Chemical Sciences, and Centre for Advanced Functional Materials, Indian Institute of Science Education and Research (IISER) Kolkata, Mohanpur - 741246, India*
[2]*Theoretical Sciences Unit, School of Advanced Materials, Jawaharlal Nehru Centre for Advanced Scientific Research (JNCASR), Bangalore 560064, India*

§ Equal contribution
* Email for correspondence: sayanb@iiserkol.ac.in

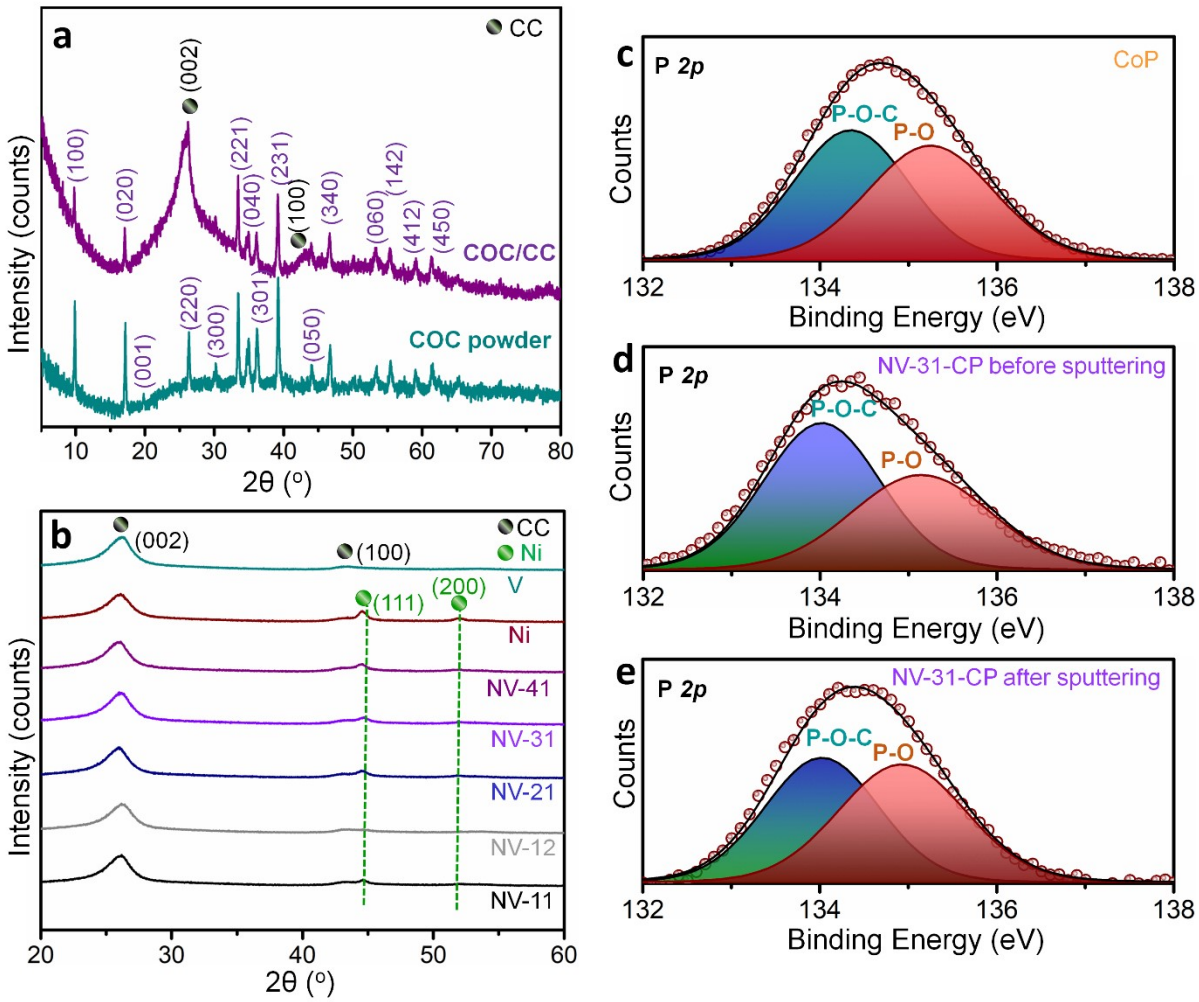

Figure S1. XRD patterns of (a) $Co(OH)_{1.0}(CO_3)_{0.5}.xH_2O$ (COC) NW powder and COC/CC, and (b) NV-11, NV-12, NV-21, NV-31, NV-41, Ni and V. XPS plots of P *2p* level for (c) CoP, (d) NV-31-CP (before 20 nm Ar^+ sputtering) and (e) NV-31-CP (after sputtering).

Table S1. ICP-OES stoichiometric data of the electrocatalysts.

Catalyst	Elemental ratio obtained from ICP-OES		
	Ni:V	Co:P	Ni:Co
NV-11	1.5:1	--	--
NV-12	1.2:2	--	--
NV-21	2.1:1	--	--
NV-31	3.4:1	--	--
NV-41	4.2:1	--	--
NV-21-CP	2.1:1	1:2.2	1.4:1
NV-31-CP	3.4:1	1:2.3	1.5:1

CoP	--	1:2.1	--

Table S2. The fitted XPS parameters of the electrocatalysts supported on carbon cloth (CC).

Catalysts	**Binding energy (eV)**			**Relative fractions**		
	Ni^{O}	**Ni^{2+}**	**Ni^{3+}**	**% Ni^{0}**	**% Ni^{2+}**	**% Ni^{3+}**
NV-31/CC	852.8	853.7	856.0	36.8	11.4	51.7
NV-31-CP/CC (before sputtering)	853.0	853.9	856.9	8.0	21.8	70.1
NV-31-CP/CC (after sputtering)	853.2	854.1	857.1	11.2	21.9	66.9
	Co^{2+}	**Co^{3+}**	**$Co^{\delta+}$** (δ>3)	**% Co^{2+}**	**% Co^{3+}**	**% $Co^{\delta+}$**
CoP/CC	782.3	779.6	783.9	50.6	2.3	47.1
NV-31-CP/CC (before sputtering)	781.8	779.2	783.8	49.7	6.6	43.7
NV-31-CP/CC (after sputtering)	782.2	779.1	783.8	64.6	1.2	34.1

	Binding energy (eV)				**Relative fractions**			
	V^{2+}	**V^{3+}**	**V^{4+}**	**V^{5+}**	**% V^{2+}**	**%V^{3+}**	**%V^{4+}**	**%V^{5+}**
NV-31/CC	514.1	515.2	516.4	517.3	6.7	22.3	30.7	40.3
NV-31-CoP/CC (before sputtering)	514.3	515.5	516.7	518.0	7.2	19.9	31.7	41.2
NV-31-CP/CC (after sputtering)	514.3	515.5	516.7	517.8	9.1	16.7	40.0	34.2

	Binding energy (eV)			**Relative fractions**		
	LO*	**M-OH****	**S-H_2O*****	**% LO**	**% M-OH**	**% S-H_2O**
CoP/CC	--	531.9	533.0	--	9.65	90.35
NV-31/CC	530.3	531.5	533.0	36.55	54.21	9.24
NV-31-CP/CC (before sputtering	--	532.0	533.0	--	32.7	67.2

NV-31-CP/CC (after sputtering)	--	532.0	532.9	--	20.6	79.3
	Binding energy (eV)			**Relative fractions**		
	P-O-C	**P-O**		**% P-O-C**	**% P-O**	
CoP/CC	134.3	135.2		50.7	49.3	
NV-31-CP/CC (before sputtering)	134.0	135.1		56.4	43.6	
NV-31-CP/CC (after sputtering)	134.0	135.0		48.6	51.4	

*LO: lattice oxygen, **M-OH: metal hydroxide, ***S-H_2O: surface adsorbed H_2O

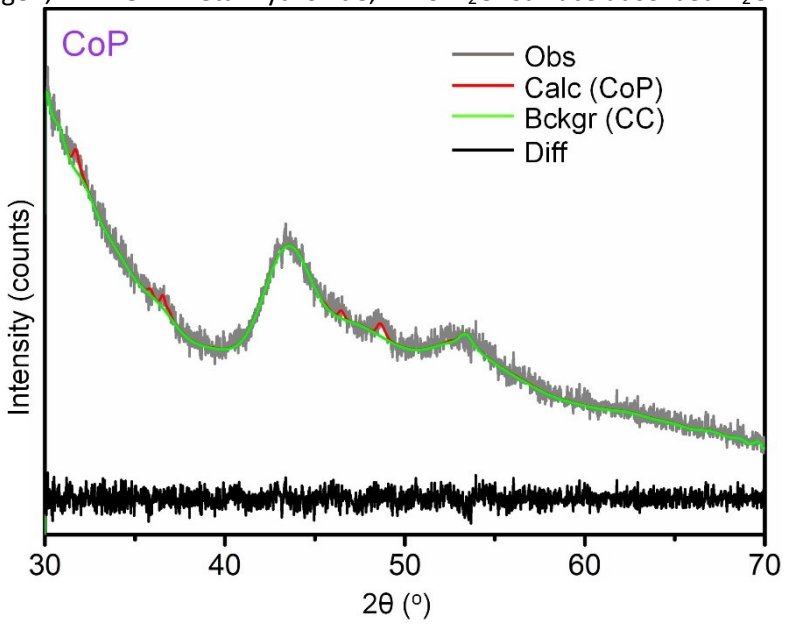

Figure S2. Rietveld refined XRD pattern of CoP. The legends: *diff* (difference plot between observed and calculated patterns); *Obs* (observed pattern); *Calc* (calculated pattern); *Bckgr* (background plot). Since CoP NWs were grown on carbon cloth (CC), the carbon reflections overshadow those from CoP. Hence, the carbon reflections were considered in the background while fitting the XRD pattern.

Table S3. XRD-Rietveld refinement parameters of CoP.

Sample	**Crystal structure Space group**	**Lattice parameters (Å)**	**Angles (°)**	**Volume (Å³)**	**Fitting parameters**
CoP	Orthorhombic *Pbnm*	a = 5.577, b = 5.009, c = 3.269	$\alpha = \beta = \gamma = 90^{O}$	91.3	χ^2 = 0.84 GOF = 0.91 R_{wp} = 2.22

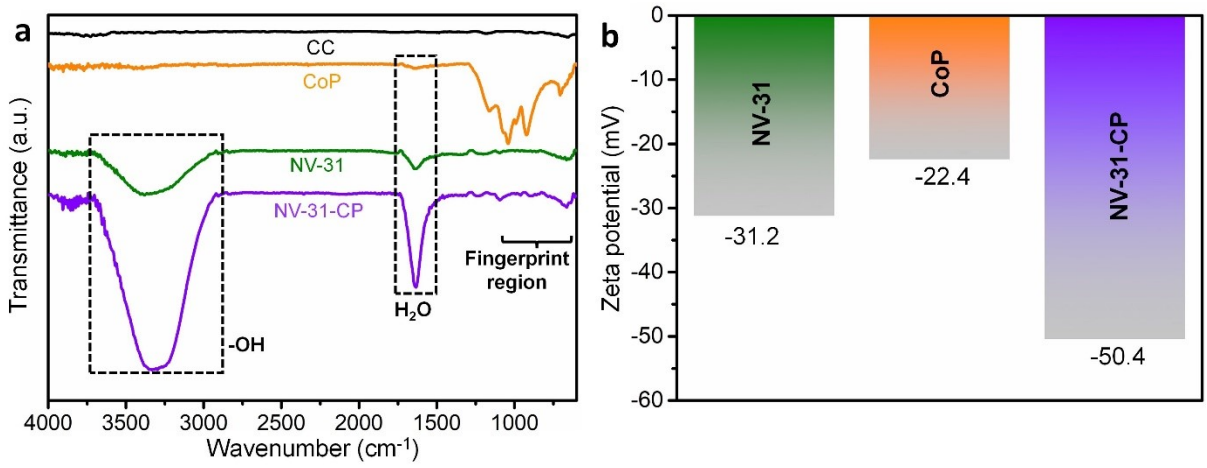

Figure S3. (a) FTIR spectra and (b) Zeta potential bar plots of NV-31, CoP and NV-31-CP.

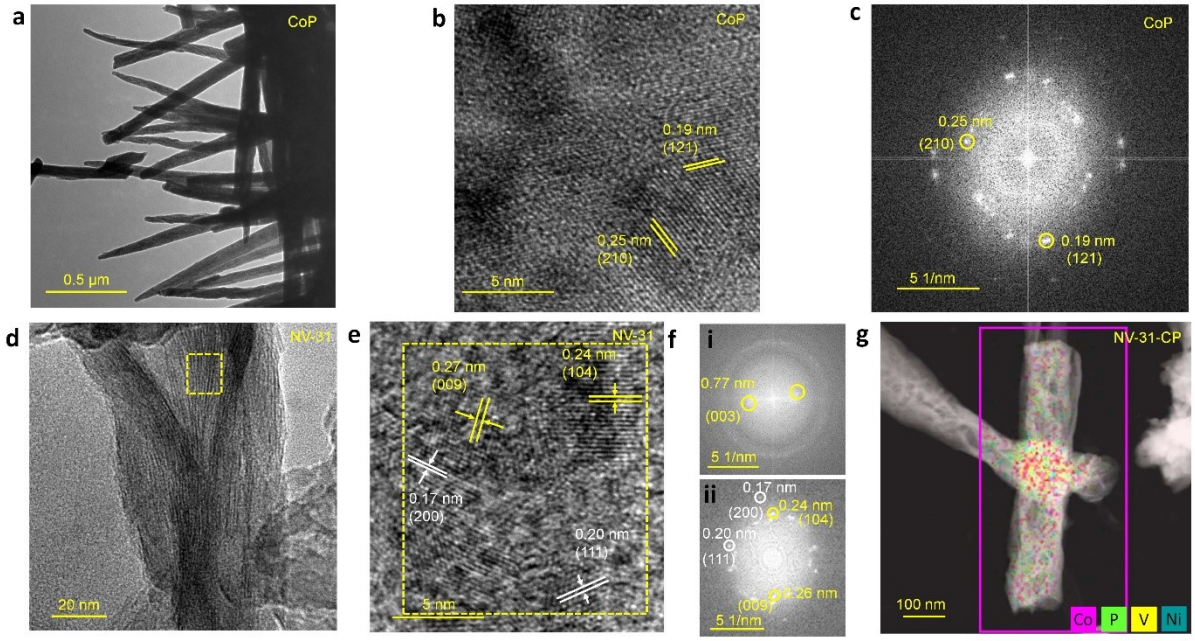

Figure S4. (a) Low and (b) high resolution TEM images, and (c) FFT pattern of CoP. (d) Low and (e) high resolution TEM images, and (f) FFT patterns of NV-31. Regions (i) and (ii) in panel (f) are from two locations indicated by yellow rectangles in panel (d) and (e), respectively. (g) HAADF-STEM elemental mapping of NV-31-CP.

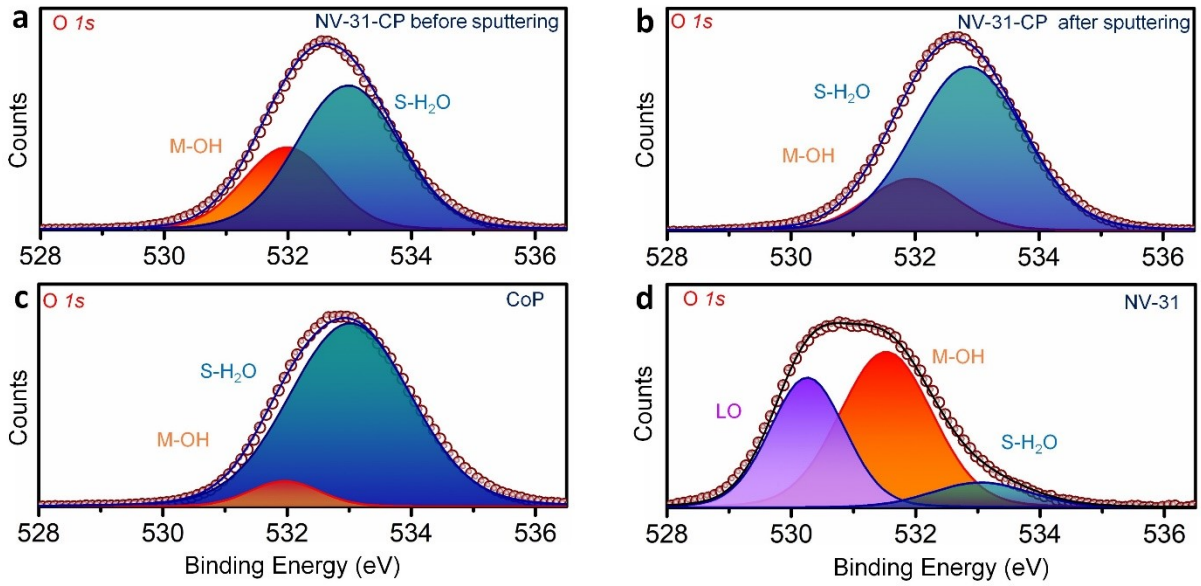

Figure S5. XPS plots of O *1s* level for (a) NV-31-CP before Ar^+ ion sputtering, (b) NV-31-CP after Ar^+ ion sputtering, (c) CoP and (d) NV-31.

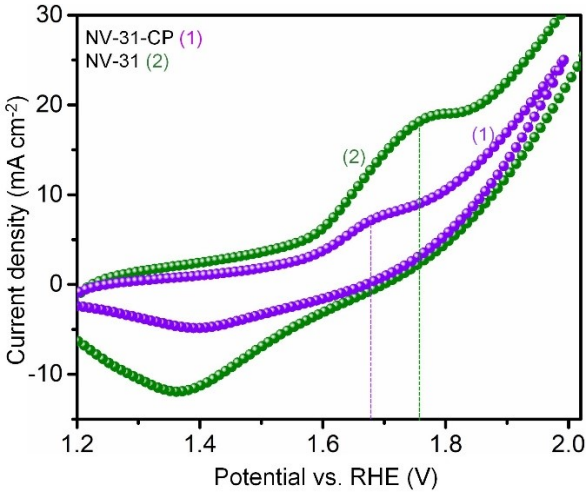

Figure S6. CV plots for NV-31 and NV-31-CP in PBS medium.

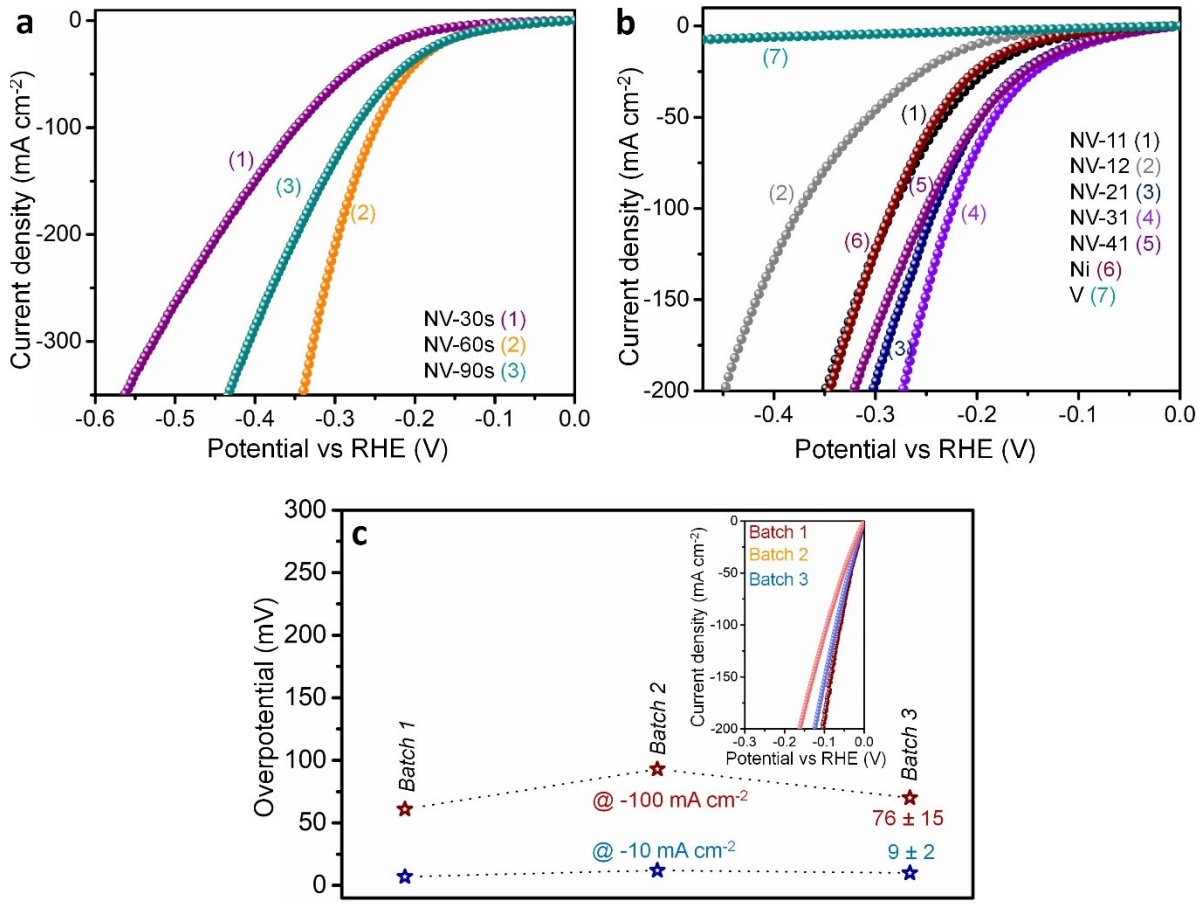

Figure S7. (a) LSV polarization curves for NV-30s (R_s = 5.8 Ω), NV-60s (R_s = 4.8 Ω), and NV-90s (R_s = 5.9 Ω). 30s, 60s and 90s indicate the time of electrodeposition of NiV-LDH on CC. (b) LSV polarization curves for NV-11 (R_s = 6.6 Ω), NV-12 (R_s = 6.6 Ω), NV-21 (R_s = 8.1 Ω), NV-31 (R_s = 4.8 Ω), NV-41 (R_s = 4.8 Ω), Ni (R_s = 6.1 Ω) and V (R_s = 5.5 Ω). (c) Overpotential scatter plots at -10, and -100 mA cm^{-2} current densities of 20% Pt/C fabricated in three batches. Inset shows the corresponding LSV plots: R_s (batch 1) = 5.3 Ω, R_s (batch 2) = 5.1 Ω, and R_s (batch 3) = 5.1 Ω.

Table S4. Solution resistance (R_s) values obtained during the LSV polarization experiments for the HER electrocatalysts in different media.

Electrolyte	R_s (Ω)				
	NV-31-CP	**NV-31**	**CoP**	**20% Pt/C**	**CC**
1M KOH	4.6	4.8	5.5	5.3	4.2
0.5M H_2SO_4	5.2	4.7	6.3	4.6	4.9
0.1M PBS	26	31.4	33	32.3	26

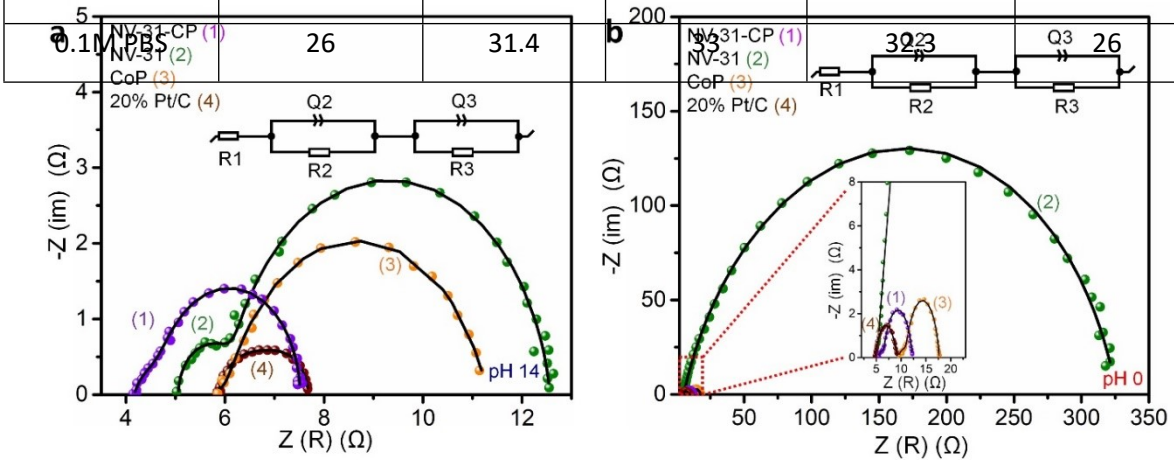

Figure S8. Fitted Nyquist plots for NV-31, CoP and NV-31-CP and 20% Pt/C in (a) 1M KOH at -1.15 V vs. Hg/HgO (1M NaOH), and (b) 0.5M H_2SO_4 at -0.4V vs. saturated calomel electrode. Insets show the zoom in plots, and the corresponding equivalent circuits. Filled circles represent the experimental data and black lines represent the fitted plot for each catalyst.

Table S5. EIS parameters obtained for the HER electrocatalysts in different media.

Electrolyte	Catalyst	R_s (Ω)	R_{CT1} (Ω)	R_{CT2} (Ω)
1M KOH (pH = 14)	NV-31-CP	4.2	0.7	2.7
	NV-31	5	1.0	6.5
	CoP	5.7	4.8	0.8
	20% Pt/C	5.8	0.6	0.8
0.5M H_2SO_4 (pH = 0)	NV-31-CP	5.5	1.1	5.7
	NV-31	5.1	198	123
	CoP	9.4	6.4	1.8
	20% Pt/C	4.6	1.8	2.8
0.1M PBS (pH = 7)	NV-31-CP	36.6	14.0	--
	NV-31	36.3	34.0	--
	CoP	35.9	49.9	--
	20% Pt/C	37.7	10.1	--

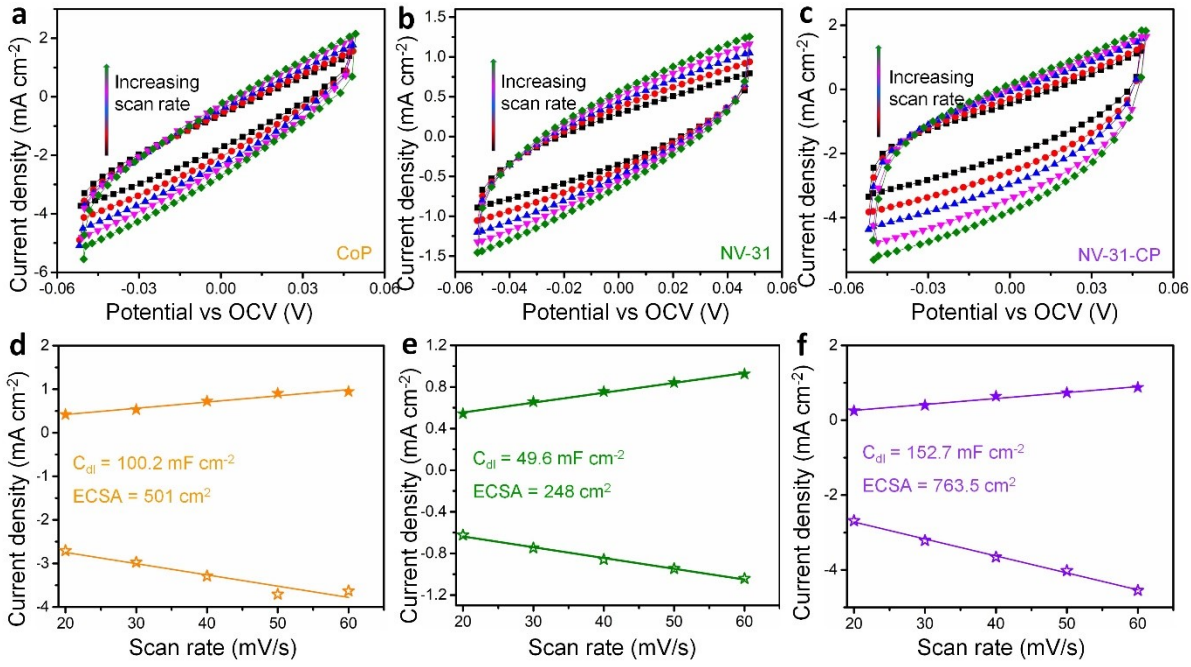

Figure S9. ECSA determination in 1M KOH. CV plots of (a) CoP, (b) NV-31, and (c) NV-31-CP at different scan rates. Plots of current density (recorded at a fixed potential) as a function of scan rate for (d) CoP, (e) NV-31, and (f) NV-31-CP.

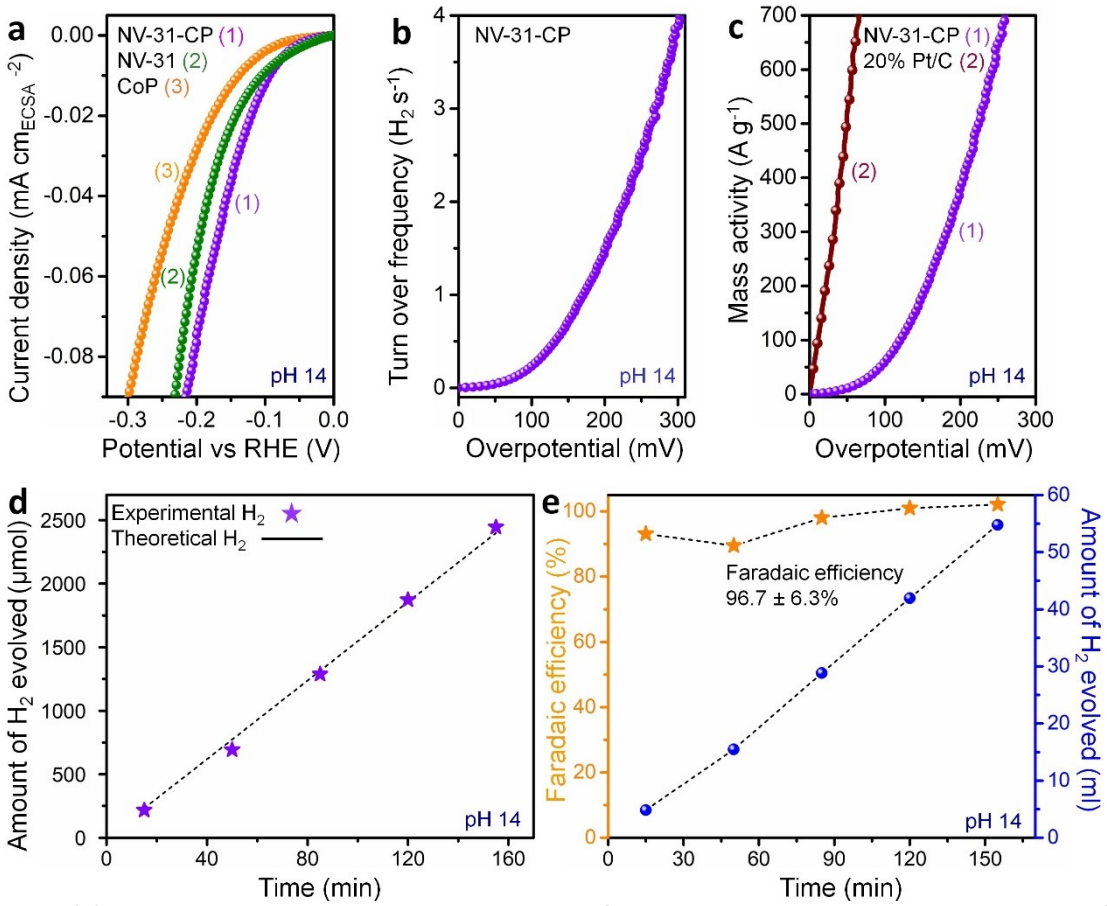

Figure S10. (a) ECSA normalized LSV polarization curves for NV-31, CoP and NV-31-CP in 1M KOH. (b) TOF of NV-31-CP in 1M KOH. (c) The mass activity of NV-31-CP and 20% Pt/C in 1M KOH. (d) Time dependent evolution of H_2 (µmol). (e) Determination of Faradaic efficiency of NV-31-CP electrocatalyst from the evolved H_2 (ml) in 1M KOH at -160 mV vs RHE.

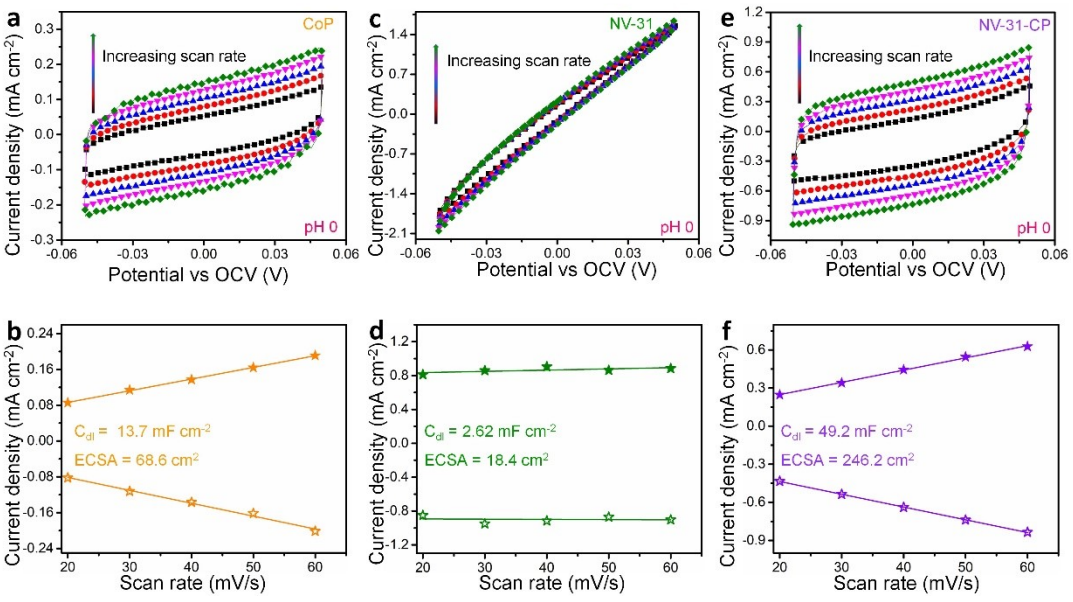

Figure S11. ECSA determination in 0.5M H_2SO_4. CV plots of (a) CoP, (b) NV-31 and (c) NV-31-CP at different scan rates. Plots of current density (recorded at a fixed potential) as a function of scan rate for (d) CoP, (e) NV-31 and (f) NV-31-CP.

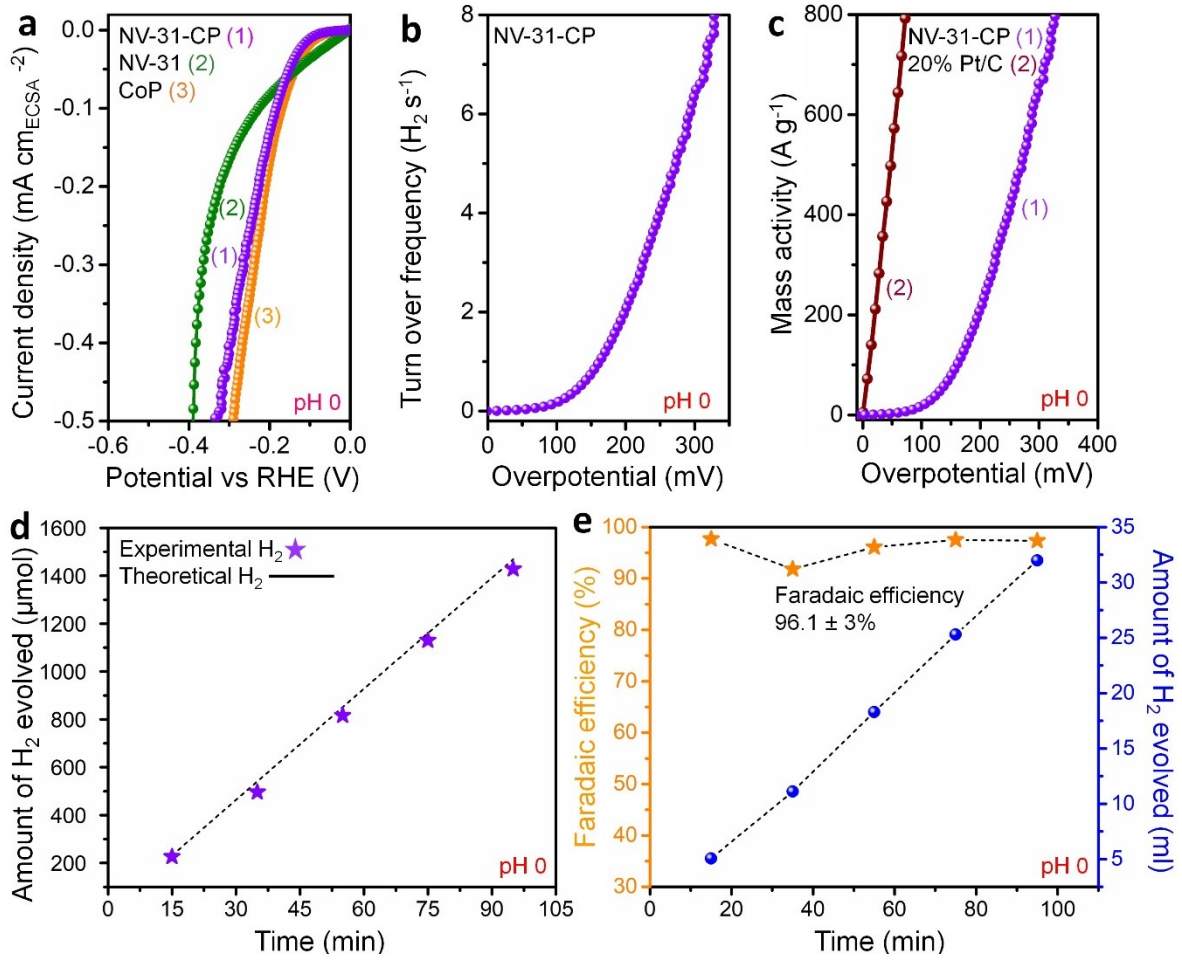

Figure S12. (a) ECSA normalized LSV polarization curves for NV-31, CoP and NV-31-CP in 0.5M H_2SO_4. (b) TOF of NV-31-CP in 0.5M H_2SO_4. (c) The mass activity of NV-31-CP and 20% Pt/C in 0.5M H_2SO_4. (d) Time dependent evolution of H_2 (µmol). (e) Determination of Faradaic efficiency of NV-31-CP electrocatalyst from the evolved H_2 (ml) in 0.5M H_2SO_4 at -202 mV vs. RHE.

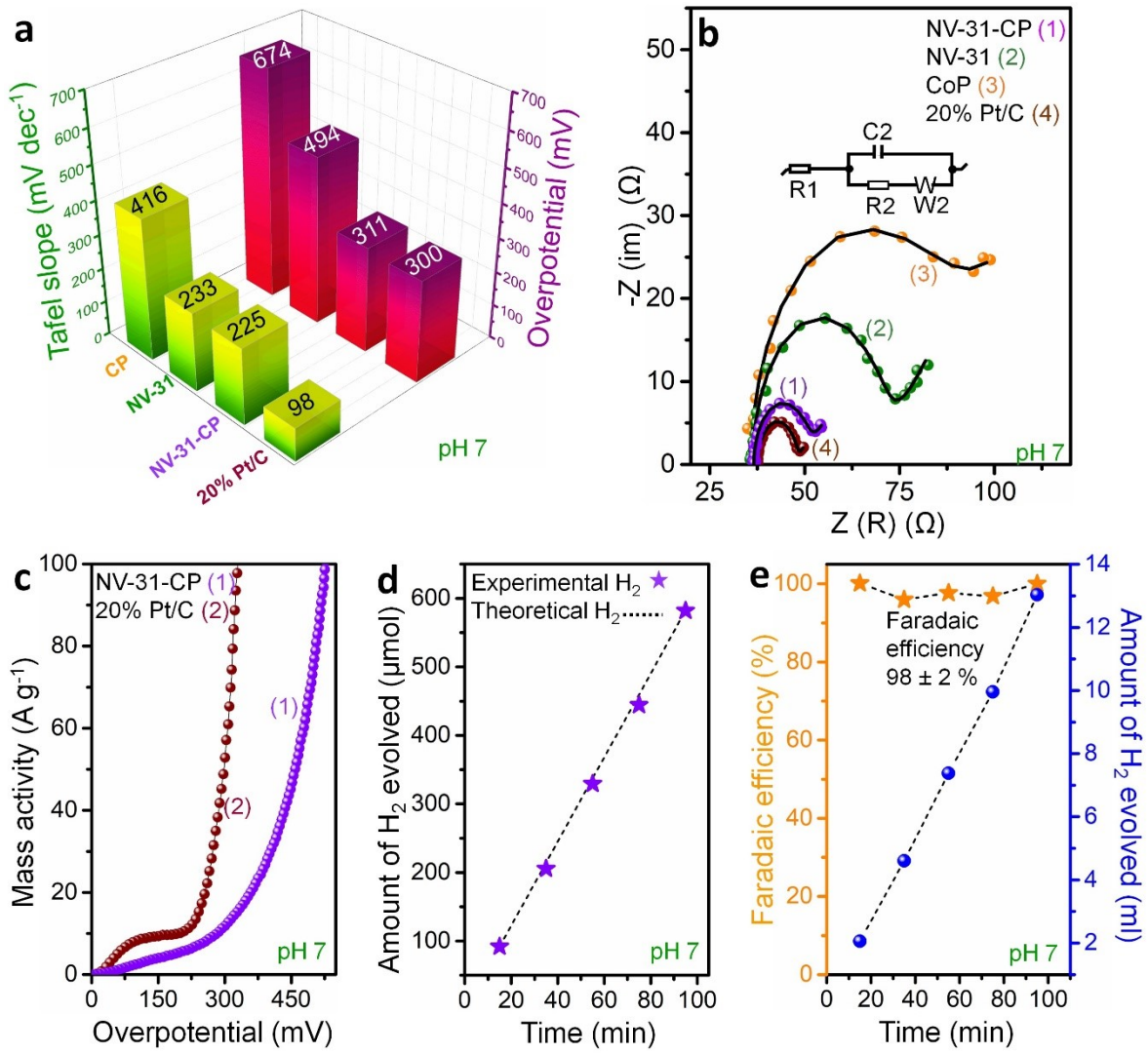

Figure S13. (a) Bar plots of Tafel slopes and overpotentials, and (b) fitted Nyquist plots of NV-31, CoP, NV-31-CP and 20% Pt/C in PBS medium at -1.2 V vs. Ag/AgCl (1M KCl). Inset shows the corresponding equivalent circuit. Filled circles represent experimental data and black lines represent the fitted data for each catalyst. (c) The mass activity of NV-31-CP and 20% Pt/C in PBS medium. (d) Time dependent evolution of H_2 (µmol). (e) Determination of Faradaic efficiency of NV-31-CP electrocatalyst from the evolved H_2 (ml) in PBS medium at -554 mV vs. RHE.

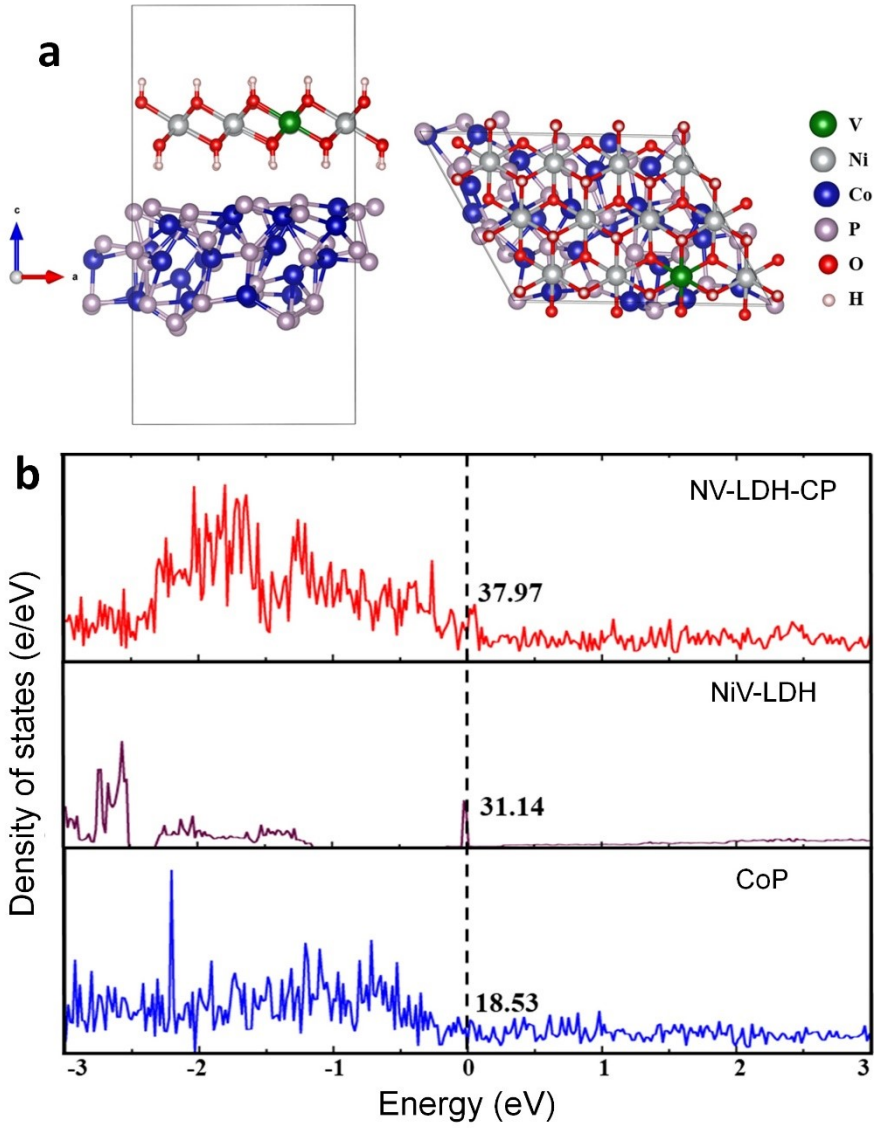

Figure S14. (a) Top and side views of NV-LDH - CP. (b) The DOS of CoP, NiV-LDH and NV-LDH - CP. Fermi energy is denoted by a dashed line.

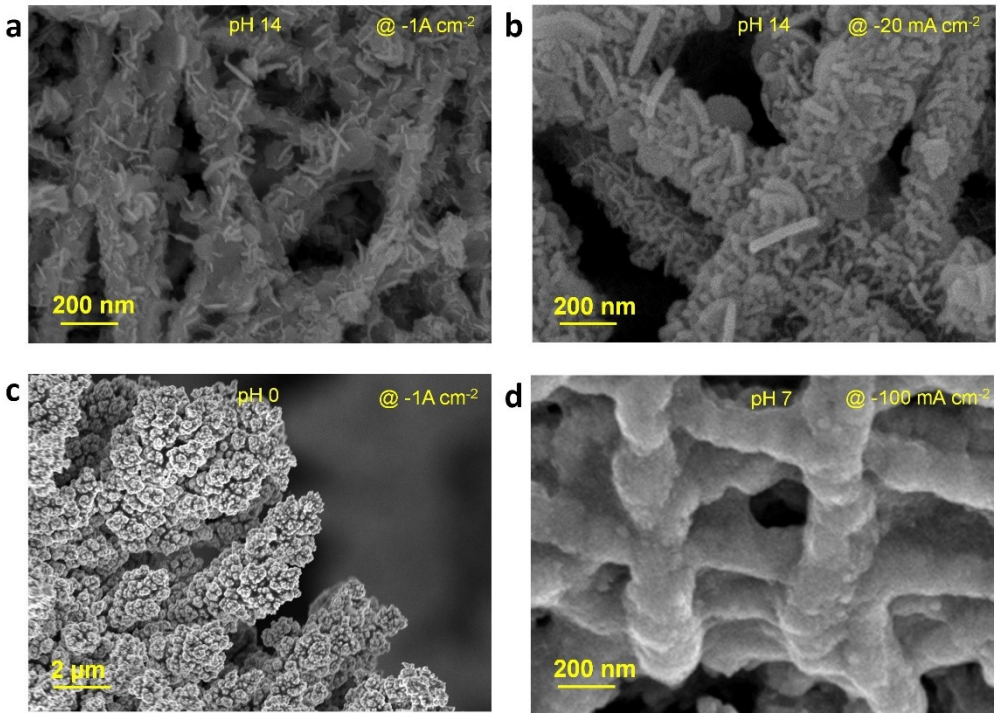

Figure S15. FESEM images of the NV-31-CP/CC electrode after the 200h stability test with Pt wire counter electrode in (a) 1M KOH by applying -1A cm^{-2} current density, (b) 1 M KOH by applying -20 mA cm^{-2}, (c) 0.5M H_2SO_4 by applying -1 A cm^{-2}, and (d) 0.1M PBS by applying -100 mA cm^{-2}.

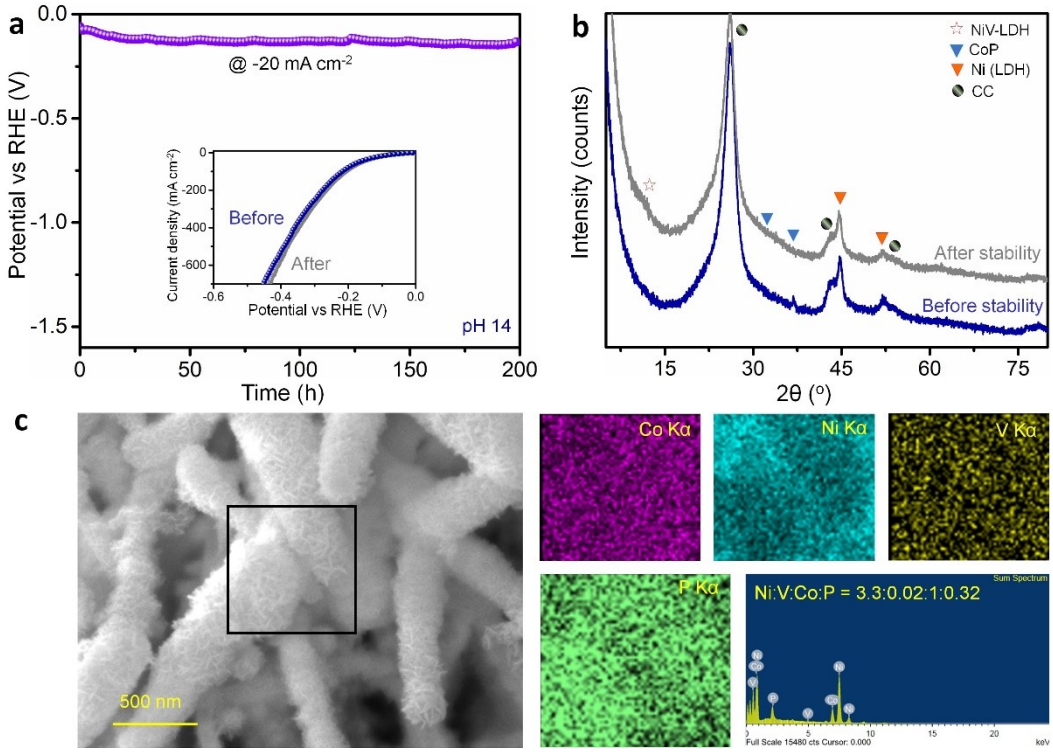

Figure S16. (a) Stability test of NV-31-CP/CC in 1M KOH at an applied current density of -20 mA cm^{-2} with Pt wire counter electrode. Inset shows the LSV polarization curve before and after the stability test (R_s = 3.8 Ω). (b) XRD patterns of the electrode before and after the stability test. (c) Elemental mapping and EDX spectrum after the stability test from the selected region of the FESEM image of NV-31-CP.

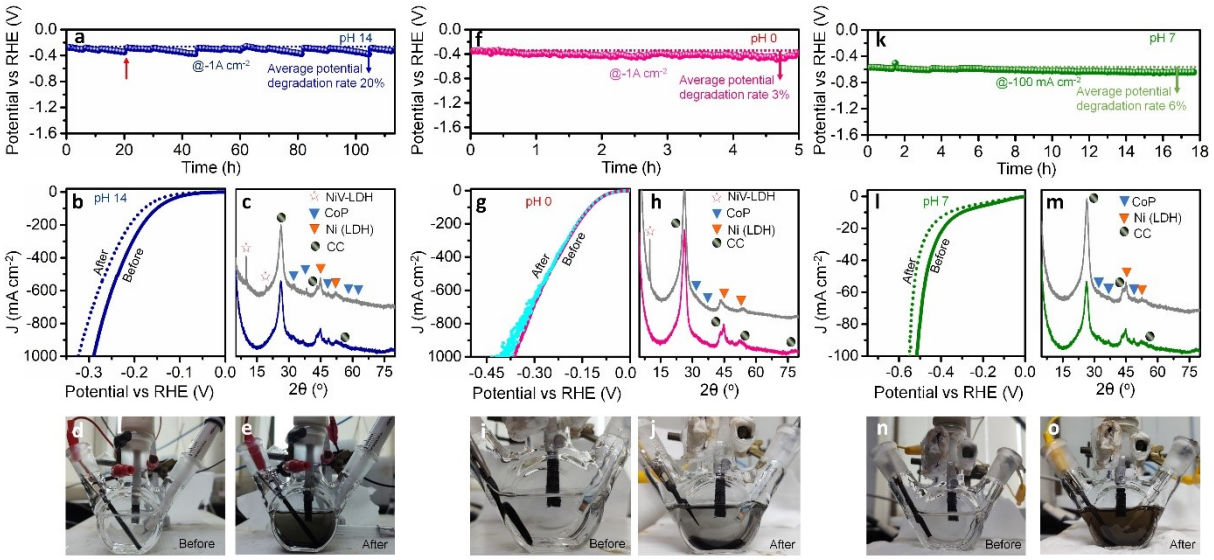

Figure S17. HER operational stability tests of NV-31-CP heterostructure at all pH with graphite rod counter electrode. (a) Chronopotentiometry at -1 A cm^{-2} for 113 h in 1M KOH (R_s = 4.3 Ω), along with (b) LSV plots (R_s = 4.0 Ω), (c) XRD patterns, and (d, e) digital images before and after the stability test. (f) Chronopotentiometry at -1 A cm^{-2} for 5 h in 0.5M H_2SO_4 (R_s = 5.5 Ω), along with (g) LSV plots (R_s = 5.5 Ω), (h) XRD patterns, and (i, j) digital images before and after the stability test. (k) Chronopotentiometry at -100 mA cm^{-2} for 18 h in 0.1M PBS medium (R_s = 35 Ω), along with (l) LSV plots (R_s = 35 Ω), (m) XRD patterns, and (n, o) digital images before and after the stability test. The up arrow in panel (a) indicate the point of electrolyte addition in order to maintain the electrode area.

Table S6. Comparison of the reported LDH-based HER electrocatalysts with NV-31-CP.

Sl. No	Catalyst	η (mV) *-10 mA cm^{-2}*	η (mV) *-100 mA cm^{-2}*	Electrolyte	Substrate	Stability (h)	Ref
1	NiFeRu-LDH	29	-	1M KOH	NF*	10	S1
2	NF@NiFe LDH/CeO_x	154	267	1M KOH	NF	20	S2
3	e-ICLDH@GDY/NF	43	215	1M KOH	NF	80	S3
4	$NiFe_2O_4$/NiFe LDH/NF	101	229	1M KOH	NF	20	S4
5	FeNi@FeNi	127	253@-50	1M KOH	NF	30	S5
6	Ni@NiFe LDH	92	233	1M KOH	NF	24	S6
7	v-NiFe LDH	87	-	1M PBS	NF	100	S7
8	$CoNiSe_2$@CoNi-LDHs/NF	106	-	1M KOH	NF	30	S8
9	CoFeCo PBA	155	330	1M KOH	CC**	50	S9
10	Rh/NiFeRh-LDH	57	-	1M KOH	NF	6	S10
11	V-Ce/CoFe LDH	73 212	-	1M KOH 1M PBS	NF	60	S11
12	Rh-doped CoFe-LDH	28	188@-600	1M KOH	NF	10	S12
13	Ru-CoV-LDH@NF	32	-	1M KOH	NF	45	S13
14	Ru_1/D-NiFe LDH	18	61	1M KOH	NF	100	S14
15	NV-31-CP/CC	55 93 311	133 173 --	1M KOH 0.5M H_2SO_4 0.1M PBS	CC	200	*This work*

* NF- Nickel Foam; **CC- Carbon Cloth

Table S7. Comparison of the reported CoP-based HER catalyst with NV-31-CP.

Sl. No	Catalyst	η (mV) *-10 mA cm^{-2}*	η (mV) *-100 mA cm^{-2}*	Electrolyte	Substrate	Stability (h)	Ref
1	CoP/CC	209 106 67	-- -- 204	1M KOH 1M PBS 0.5M H_2SO_4	CC*	5000 CV	S15
2	V-CoP/CC	71 123 47	-	1M KOH 1M PBS 0.5M H_2SO_4	CC	25	S16
3	Ce doped CoP	92 54	161- 120	1M KOH 0.5M H_2SO_4	Ti plates	10	S17
4	Fe-CoP UNSs	67	148	1M KOH	NF**	50	S18
5	CoP NWs	-	244	1M KOH	Cobalt foam	48	S19
6	CoP/Co_2P	103 99	155@50 mA cm^{-2} 146@50 mA cm^{-2}	1M KOH 0.5M H_2SO_4	GC	<8	S20
7	CoP/Ni_5P_4/CoP	71 33	140 85	1M KOH 0.5M H_2SO_4	NF	27	S21
8	$NiCo_2$–B–P	78	-	1M KOH	NF	9	S22
9	B-CoP/CNT	56 79 39	-	1M KOH 1M PBS 0.5M H_2SO_4	GC***	100	S23
10	CoP/Co-MOF	34 49 27	-	1M KOH 1M PBS 0.5M H_2SO_4	CFP****	16.5	S24
11	CoP-InNC@CNT	159 153	-	1M KOH 0.5M H_2SO_4	GC	20	S25
12	$NiCo_{16-x}P_x$	88	-	1M KOH	GC/CFP	10	S26
	NV-31-CP/CC	55 93 311	133 173 --	1M KOH 0.5M H_2SO_4 0.1M PBS	CC	200	*This work*

*CC- Carbon Cloth, **NF- Nickel Foam, ***GC-Glassy Carbon, ****CFP-Carbon Fiber Paper

Table S8. Comparison of the reported self-supported electrodes for HER with NV-31-CP/CC.

Sl. No	Catalyst	η (mV) *-10 mA cm^{-2}*	η (mV) *-100 mA cm^{-2}*	Electrolyte	Substrate	Stability (h)	Ref
1	RuP/CC RuP_2/CC	13 33	53 -	1M KOH	CC*	20	S27
2	N-Co_3O_4@C@NF	42	-	1M KOH	NF**	60	S28
4	VC@NC/CC	151 130	317 238	1M KOH 0.5M H_2SO_4	CC	20	S29
5	CoFe-P/NF	83	180	1M KOH	NF	25	S30
6	Mo_2C-3 M $Ni(NO_3)_2$/CFP	56	-	0.5M H_2SO_4	CFP***	35	S31
7	Ni_xP/NF	71	153	1M KOH	NF	40	S32
8	Cu-m/Cu-W/NiCo-LDH	15 27	72 112	1M KOH 0.5M H_2SO_4	Cu-m	120 50	S33
9	NiCoP@NC NA/NF	37 34	186 150	1M KOH 0.5M H_2SO_4	NF	22	S34
11	TiC@MoS_2	127	160 @50 mA cm^{-2}	0.5M H_2SO_4	TiC	24	S35
12	PS-Cu	121 261 182	534 568 340	1M KOH 1M PBS 0.5M H_2SO_4	Cu-m****	30	S36
13	WP-W_2C/W	43	139 560 @1000 mA cm^{-2}	1M KOH	W foil	60	S37
15	NiCo-LDH−1T-WS_2/CC	134	-	1M KOH	CC	60	S38
16	Cu@(Ni/NiO)	67	--	1M KOH	MC*****	24	S39
17	Ni_2P/V_2O_{3-x}	59	--	1M KOH	NF	100	S40
	NV-31-CP/CC	55 93 311	133 173 --	1M KOH 0.5M H_2SO_4 PBS	CC	200	*This work*

*CC- Carbon Cloth, **NF- Nickel Foam, ***CFP- Carbon Fiber Paper, ****Cu-m- Cu mesh, *****MC-

Metallic Glass

Supporting References

(S1) G. Chen, T. Wang, J. Zhang, P. Liu, H. Sun, X. Zhuang, M. Chen and X. Feng, *Adv. Mater.*, 2018, **30**, 1–7.

(S2) X. Wang, Y. Yang, L. Diao, Y. Tang, F. He, E. Liu, C. He, C. Shi, J. Li, J. Sha, S. Ji, P. Zhang, L. Ma and N. Zhao., *ACS Appl. Mater. Interfaces*, 2018, **10**, 35145–35153.

(S3) L. Hui, Y. Xue, B. Huang, H. Yu, C. Zhang, D. Zhang, D. Jia, Y. Zhao, Y. Li, H. Liu and Y. Li, *Nat. Commun.*, 2018, **9**, 1–11.

(S4) Z. Wu, Z. Zou, J. Huang and F. Gao, *ACS Appl. Mater. Interfaces*, 2018, **10**, 26283–26292.

(S5) K. Huang, R. Dong, C. Wang, W. Li, H. Sun and B. Geng, *ACS Sustain. Chem. Eng.*, 2019, **7**, 15073–15079.

(S6) Z. Cai, X. Bu, P. Wang, W. Su, R. Wei, J. C. Ho, J. Yang and X. Wang, *J. Mater. Chem. A*, 2019, **7**, 21722–21729.

(S7) Z. Yuan, S. M. Bak, P. Li, Y. Jia, L. Zheng, Y. Zhou, L. Bai, E. Hu, X. Q. Yang, Z. Cai, Y. Sun and X. Sun, *ACS Energy Lett.*, 2019, **4**, 1412–1418.

(S8) Y. Yang, W. Zhang, Y. Xiao, Z. Shi, X. Cao, Y. Tang and Q. Gao, *Appl. Catal. B Environ.*, 2019, **242**, 132–139.

(S9) B. Singh, O. Prakash, P. Maiti, P. W. Menezes and A. Indra, *Chem. Commun.*, 2020, **56**, 15036–15039.

(S10) B. Zhang, C. Zhu, Z. Wu, E. Stavitski, Y. H. Lui, T. H. Kim, H. Liu, L. Huang, X. Luan, L. Zhou, K. Jiang, W. Huang, S. Hu, H. Wang and J. S. Francisco, *Nano Lett.*, 2020, **20**, 136–144.

(S11) S. Liu, J. Zhu, M. Sun, Z. Ma, K. Hu, T. Nakajima, X. Liu, P. Schmuki and L. Wang, *J. Mater. Chem. A*, 2020, **8**, 2490–2497.

(S12) K. Zhu, J. Chen, W. Wang, J. Liao, J. Dong, M. O. L. Chee, N. Wang, P. Dong, P. M. Ajayan, S. Gao, J. Shen and M. Ye, *Adv. Funct. Mater.*, 2020, **30**, 1–10.

(S13) W. Li, B. Feng, L. Yi, J. Li and W. Hu, *ChemSusChem*, 2021, **14**, 730–737.

(S14) P. Zhai, M. Xia, Y. Wu, G. Zhang, J. Gao, B. Zhang, S. Cao, Y. Zhang, Z. Li, Z. Fan, C. Wang, X. Zhang, J. T. Miller, L. Sun and J. Hou, *Nat. Commun.*, 2021, **12**, 1–11.

(S15) J. Tian, Q. Liu, A. M. Asiri and X. Sun, *J. Am. Chem. Soc.*, 2014, **136**, 7587–7590.

(S16) X. Xiao, L. Tao, M. Li, X. Lv, D. Huang, X. Jiang, H. Pan, M. Wang and Y. Shen, *Chem. Sci.*, 2018, **9**, 1970–1975.

(S17) W. Gao, M. Yan, H. Y. Cheung, Z. Xia, X. Zhou, Y. Qin, C. Y. Wong, Y. Qu, C. R. Chang and J. C. Ho, *Nano Energy*, 2017, **38**, 290–296.

(S18) Y. Li, F. Li, Y. Zhao, S. N. Li, J. H. Zeng, H. C. Yao and Y. Chen, *J. Mater. Chem. A*, 2019, **7**, 20658–20666.

(S19) W. Li, X. Gao, D. Xiong, F. Xia, J. Liu, W. G. Song, J. Xu, S. M. Thalluri, M. F. Cerqueira, X. Fu and L. Liu, *Chem. Sci.*, 2017, **8**, 2952–2958.

(S20) L. Chen, Y. Zhang, H. Wang, Y. Wang, D. Li and C. Duan, *Nanoscale*, 2018, **10**, 21019–21024.

(S21) I. K. Mishra, H. Zhou, J. Sun, F. Qin, K. Dahal, J. Bao, S. Chen and Z. Ren, *Energy Environ. Sci.*, 2018, **11**, 2246–2252.

(S22) M. Liu, Q. He, S. Huang, W. Zou, J. Cong, X. Xiao, P. Li, J. Cai and L. Hou, *ACS Appl. Mater. Interfaces*, 2021, **13**, 9932–9941.

(S23) E. Cao, Z. Chen, H. Wu, P. Yu, Y. Wang, F. Xiao, S. Chen, S. Du, Y. Xie, Y. Wu and Z. Ren, *Angew. Chem. Int. Ed.*, 2020, **59**, 4154–4160.

(S24) T. Liu, P. Li, N. Yao, G. Cheng, S. Chen, W. Luo and Y. Yin, *Angew. Chem. Int. Ed.*, 2019, **58**, 4679–4684.

(S25) L. Chai, Z. Hu, X. Wang, Y. Xu, L. Zhang, T. T. Li, Y. Hu, J. Qian and S. Huang, *Adv. Sci.*, 2020, **7**, 1903195.

(S26) Y. Zhao, J. Zhang, Y. Xie, B. Sun, J. Jiang, W. J. Jiang, S. Xi, H. Y. Yang, K. Yan, S. Wang, X. Guo, P. Li, Z. Han, X. Lu, H. Liu and G. Wang, *Nano Lett.*, 2021, **21**, 823–832.

(S27) R. Ge, S. Wang, J. Su, Y. Dong, Y. Lin, Q. Zhang and L. Chen, *Nanoscale*, 2018, **10**, 13930–13935.

(S28) Y. Ha, L. Shi, Z. Chen and R. Wu, *Adv. Sci.*, 2019, **6**, 1900272.

(S29) L. Guo, Y. Liu, X. Teng, Y. Niu, S. Gong and Z. Chen, *ChemSusChem*, 2020, **13**, 3671–3678.

(S30) X. Wang, C. Wang, F. Lai, H. Sun, N. Yu and B. Geng, *ACS Appl. Nano Mater.*, 2021, **4**, 12083–12090.

(S31) Z. Hu, L. Zhang, J. Huang, Z. Feng, Q. Xiong, Z. Ye, Z. Chen, X. Li and Z. Yu, *Nanoscale*, 2021, **13**, 8264–8274.

(S32) Y. Wang, L. Liu, X. Zhang, F. Yan, C. Zhu and Y. Chen, *J. Mater. Chem. A*, 2019, **7**, 22412–22419.

(S33) S. Parvin, A. Kumar, A. Ghosh and S. Bhattacharyya, *Chem. Sci.*, 2020, **11**, 3893–3902.

(S34) B. Cao, Y. Cheng, M. Hu, P. Jing, Z. Ma, B. Liu, R. Gao and J. Zhang, *Adv. Funct. Mater.*, 2019, **29**, 1–18.

(S35) Y. Shi, D. Zheng, X. Zhang, K. Lv, F. Wang, B. Dong, S. Wang, C. Yang, J. Li, F. Yang, L. Y. Hao, L. Yin, X. Xu, Y. Xian and S. Agathopoulos, *Chem. Mater.*, 2021, **33**, 6217–6226.

(S36) W. J. Kang, Y. Feng, Z. Li, W. Q. Yang, C. Q. Cheng, Z. Z. Shi, P. F. Yin, G. R. Shen, J. Yang, C. K. Dong, H. Liu, F. X. Ye and X. W. Du, *Adv. Funct. Mater.*, 2022, **32**, 1–8.

(S37) J. Huang, C. Jian, Q. Cai, W. Hong and W. Liu, *J. Mater. Chem. A*, 2022, **10**, 10990–10997.

(S38) S. Parvin, V. Hazra, A. G. Francis, S. K. Pati and S. Bhattacharyya, *Inorg. Chem.*, 2021, **60**, 6911–6921.

(S39) Z. Li, R. Wu, Y. Wen, F. K. Chiang, X. J. Liu, J. Wang, R. Li, H. Wang, Y. Wu, S. Jiang, X. Wang and Z. P. Lu, *Nanoscale*, 2022, **14**, 325–332.

(S40) R. Li, B. Chu, J. Liu, F. Wang, Z. Chen, Q. Pang, B. Li, M. Fan and L. Dong, *ACS Sustain. Chem. Eng.*, 2022, **10**, 12262-12270.